TREM-like transcript-1 protects against inflammation-associated hemorrhage by facilitating platelet aggregation in mice and humans

A. Valance Washington,[1,2] Sébastien Gibot,[3,4] Ismael Acevedo,[1] James Gattis,[5] Laura Quigley,[2] Robert Feltz,[2] Alina De La Mota,[1] Rebecca L. Schubert,[2] Julio Gomez-Rodriguez,[6] Jun Cheng,[6] Amalia Dutra,[6] Evgenia Pak,[6] Oleg Chertov,[7] Linette Rivera,[1] Jessica Morales,[1] Jacek Lubkowski,[5] Robert Hunter,[1] Pamela L. Schwartzberg,[6] and Daniel W. McVicar[2]

[1]Laboratory of Anatomy and Cell Biology, Universidad Central del Caribe, Bayamón, Puerto Rico, USA. [2]Cancer and Inflammation Program, National Cancer Institute, Frederick, Maryland, USA. [3]Service de Réanimation Médicale, Hôpital Central, Nancy, France. [4]Groupe Choc, contrat Avenir INSERM, Faculté de Médecine, Nancy-Université, Nancy, France. [5]Macromolecular Crystallography Laboratory, National Cancer Institute, NIH, Frederick, Maryland, USA. [6]National Human Genome Research Institute, NIH, Bethesda, Maryland, USA. [7]Protein Chemistry Laboratory, Advanced Technology Program, SAIC–Frederick Inc., National Cancer Institute, Frederick, Maryland, USA.

Triggering receptor expressed on myeloid cells–like (TREM-like) transcript-1 (TLT-1), a type 1 single Ig domain orphan receptor specific to platelet and megakaryocyte α-granules, relocates to the platelet surface upon platelet stimulation. We found here that patients diagnosed with sepsis, in contrast to healthy individuals, had substantial levels of soluble TLT-1 (sTLT-1) in their plasma that correlated with the presence of disseminated intravascular coagulation. sTLT-1 bound to fibrinogen and augmented platelet aggregation in vitro. Furthermore, the cytoplasmic domain of TLT-1 could also bind ezrin/radixin/moesin family proteins, suggesting its ability to link fibrinogen to the platelet cytoskeleton. Accordingly, platelets of *Treml1*$^{-/-}$ mice failed to aggregate efficiently, extending tail-bleeding times. Lipopolysaccharide-treated *Treml1*$^{-/-}$ mice developed higher plasma levels of TNF and D-dimers than wild-type mice and were more likely to succumb during challenge. Finally, *Treml1*$^{-/-}$ mice were predisposed to hemorrhage associated with localized inflammatory lesions. Taken together, our findings suggest that TLT-1 plays a protective role during inflammation by dampening the inflammatory response and facilitating platelet aggregation at sites of vascular injury. Therefore, therapeutic modulation of TLT-1–mediated effects may provide clinical benefit to patients with hypercoagulatory conditions, including those associated with inflammation.

Introduction

Septic shock claims over 200,000 people a year in the United States and is a leading cause of morbidity and mortality. Death from sepsis occurs when the deposition of microthrombi, together with vasodilation, results in loss of perfusion, leading to multiple organ failure. Platelets play an integral part in the thrombin generation and thrombus formation that lead to organ failure and death. The morbidity of sepsis, however, begins with an inflammatory response that causes endothelial dysfunction, vascular leakage, and a subsequent systemic activation of the hemostatic system manifested as profound thrombocytopenia and disseminated intravascular coagulation (DIC) (1). This sequence of events in the development of sepsis is considered an attractive temporal point for therapeutic intervention, and thus great efforts have been put forth to define the events that regulate the inflammatory activation of the hemostatic system (2).

The triggering receptor expressed on myeloid cells (TREM) gene cluster includes several type 1, single Ig domain–containing orphan receptors clustered on human chromosome 6 and mouse chromosome 17 (3). The founding members of the TREM receptor family (TREM-1 and TREM-2) couple to the immune receptor tyrosine-based activation motif–containing receptor chain DAP12 and activate various cells of the myeloid lineage, including monocytes, macrophages, neutrophils, and dendritic cells (4, 5). In addition to DAP12-coupled receptors, the TREM gene cluster includes TREM-like transcript-1 (TLT-1) (6). Unlike TREM-1 and -2, TLT-1 does not couple to DAP12 and little is known regarding its function. Unlike other TREMs, TLT-1 has been reported only in the platelet and megakaryocyte lineage, suggesting that it plays a specific role in hemostasis and/or thrombosis and could be an attractive target for modulating platelet function (7). Along with P selectin, TLT-1 is sequestered in the platelet α-granules, and it has been demonstrated that upon platelet activation with thrombin, collagen, or LPS, it is moved to the platelet surface (7, 8).

Our recent characterization of TLT-1 demonstrated that activated platelets release a soluble fragment detectable in serum but not in plasma of healthy mice or humans (9). This finding suggests that detection of significant levels of soluble TLT-1 (sTLT-1)

Conflict of interest: The C10 anti–TLT-1 antibody used to obtain data shown in Figure 5 is covered under a provisional patent application by the NIH. D.W. McVicar, A.V. Washington, and L. Quigley are inventors on that provisional patent.

Nonstandard abbreviations used: DIC, disseminated intravascular coagulation; ERM, ezrin/radixin/moesin; GST, glutathione-*S*-transferase; His, histidine; IQR, interquartile range; ISTH, International Society on Thrombosis and Haemostasis; ROC, receiver operating characteristic; rsTLT-1, recombinant soluble TLT-1; SAPSII, Simplified Acute Physiology Score II; SOFA, Sepsis-related Organ Failure Assessment; sTLT-1, soluble TLT-1; TLT-1, TREM-like transcript-1; TREM, triggering receptor expressed on myeloid cells.

Citation for this article: *J. Clin. Invest.* **119**:1489–1501 (2009). doi:10.1172/JCI36175.

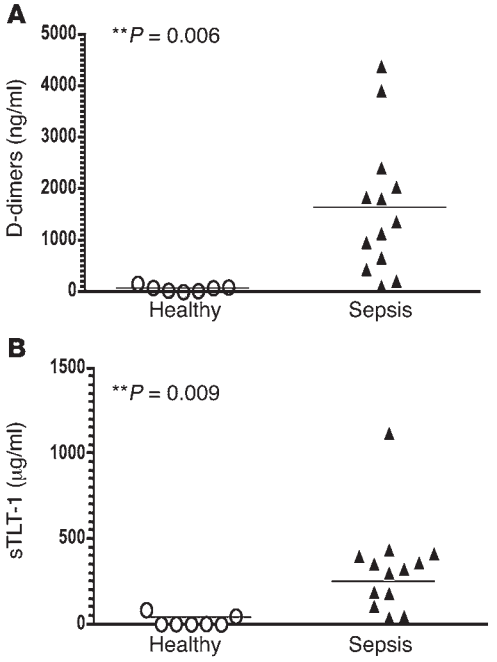

Figure 1
Elevated levels of D-dimers and sTLT-1 in patients diagnosed with sepsis. Plasma isolated from patients diagnosed with sepsis or healthy individuals was evaluated for the presence of D-dimers by ELISA (**A**) and sTLT-1 by dot blot analysis (**B**). Markers represent individual patients. Horizontal lines represent the mean. *P* values represent results from Student's *t* test.

in the plasma may serve as an important indicator of peripheral platelet activation in specific disease states. In addition, we demonstrated that blocking TLT-1 with TLT-1–specific single-chain fragment antibodies (scFv) inhibited platelet aggregation induced by low concentrations of agonists in vitro, suggesting that TLT-1 may facilitate platelet aggregation during early stages of vessel damage in vivo (10).

Here we show that patients diagnosed with sepsis have dramatically increased levels of sTLT-1 in their blood and that this level correlates with the clinical manifestation of DIC. Consistent with this finding, we demonstrate that TLT-1 augments platelet aggregation. We further demonstrate that TLT-1 binds fibrinogen and directly couples to the ezrin/radixin/moesin (ERM) family of actin-binding proteins, providing a potential mechanism for TLT-1–mediated enhancement of platelet aggregation. Accordingly, we define a defect in platelet aggregation in mice lacking TLT-1 and report the presence of sTLT-1 in the plasma of mice challenged with LPS. Lastly, we demonstrate the inability of these animals to control hemorrhage associated with inflammatory injury. Collectively, these data define TLT-1 as a regulator of hemostasis during sepsis via autocrine stimulation of platelet aggregation. Moreover, these data define TLT-1 as a potentially valuable biomarker for sepsis and imply that the circulating levels sTLT-1 represent biologically active molecules in the regulation of inflammation and thrombosis.

Results

Detection of sTLT-1 in septic patients. DIC is prominent in patients with sepsis (11). Given our previous observation of sTLT-1 in the serum but not the plasma of healthy donors, we screened for the presence of plasma sTLT-1 in a small cohort of patients diagnosed with clinical sepsis following admission to the Ruiz Arnau University Hospital (Bayamón, Puerto Rico, USA). The demographic and clinical profiles of the subjects of this initial study are listed in Supplemental Table 1 (supplemental material available online with this article; doi:10.1172/JCI36175DS1). In this initial study, 20 individuals (7 healthy and 13 admitted with the diagnosis of sepsis) were first evaluated for the presence of D-dimers, a degradation product of cross-linked fibrin, the level of which becomes elevated following fibrinolysis. Healthy individuals had a median (interquartile range [IQR]) level of 17.3 ng/ml (4.0–107.8), whereas septic individuals had a level of 1344.0 ng/ml (544.8–2224.0) D-dimers, confirming that the majority of these patients had detectable disseminated activation of their coagulation systems (Figure 1A). We then evaluated the levels of sTLT-1 in the plasma of these individuals by dot blot analysis. The median (IQR) level of sTLT-1 in patients diagnosed with sepsis was 320.7 μg/ml (145.3–403.8), while that of healthy individuals was only 0 μg/ml (0–45.0) (Figure 1B).

Correlations between sTLT-1, DIC, and survival. Based on these initial data, we conducted a longitudinal study of sTLT-1 during sepsis at the Hôpital Central. Forty-six septic shock patients were included in this study. Unlike our initial screening for sTLT-1, which included HIV-positive individuals, patients were not enrolled in this study if they were immunocompromised. All were seriously ill, as witnessed by the universal need for mechanical ventilation and vasopressor therapy. The main clinical and biological characteristics of this cohort are summarized in Supplemental Table 2. There were no differences in clinical parameters between survivors and nonsurvivors on admission. Infection originated from the lung (community-acquired pneumonia, 65%), the urinary tract (pyelonephritis, 9%), or the abdomen (peritonitis, 26%). Microbiological documentation was obtained in 32 (69.5%) patients (Supplemental Table 3). The high 28-day mortality rate (47.8%) was not unexpected, considering the elevated Simplified Acute Physiology Score II (SAPSII) and Sepsis-related Organ Failure Assessment (SOFA) score of this cohort.

Analysis of plasma sTLT-1 levels in these septic patients showed a median (IQR) sTLT-1 concentration of 36.6 (16.5–79.8) μg/ml at admission, as compared with 5.4 (0–38.4) μg/ml in 15 healthy volunteer controls ($P < 0.005$). sTLT-1 levels at admission did not differ between survivors and nonsurvivors, and we found no correlation with the SOFA score or each of its components taken individually (PaO_2/FiO_2, platelet count, bilirubinemia, mean arterial pressure, creatinemia, Glasgow coma score). Interestingly, while there was a progressive decline of sTLT-1 concentration among the survivors, nonsurvivors showed an increase in sTLT-1 levels between day 1 and day 3 (Figure 2A). Thus, the 2 populations diverged after day 3 ($P < 0.03$), with 20 of 24 survivors (83.3%) showing a decrease in sTLT-1 between day 1 and day 3 of the study. In contrast, sTLT-1 increased in all but 5 (17/22, 77.3%) nonsurvivors.

Considering the potential implications of TLT-1 in regulation of coagulation, we investigated the relationship between plasma sTLT-1 and DIC. Indeed, we found a strong correlation (Rs = 0.75; $P < 0.0001$) between sTLT-1 and DIC score, as appreciated using the International Society on Thrombosis and Haemostasis (ISTH) criteria (Figure 2B). Although no correlation was found with platelet counts or prothrombin time, sTLT-1 was strongly correlated with D-dimer levels (Rs = 0.82, $P < 0.0001$; Figure 2C). Consequently, patients suffering from DIC (DIC score > 5) had a higher plasma sTLT-1 concentration than those without DIC (Figure 2D) (12). Thus, we next sought to evaluate the usefulness of sTLT-1

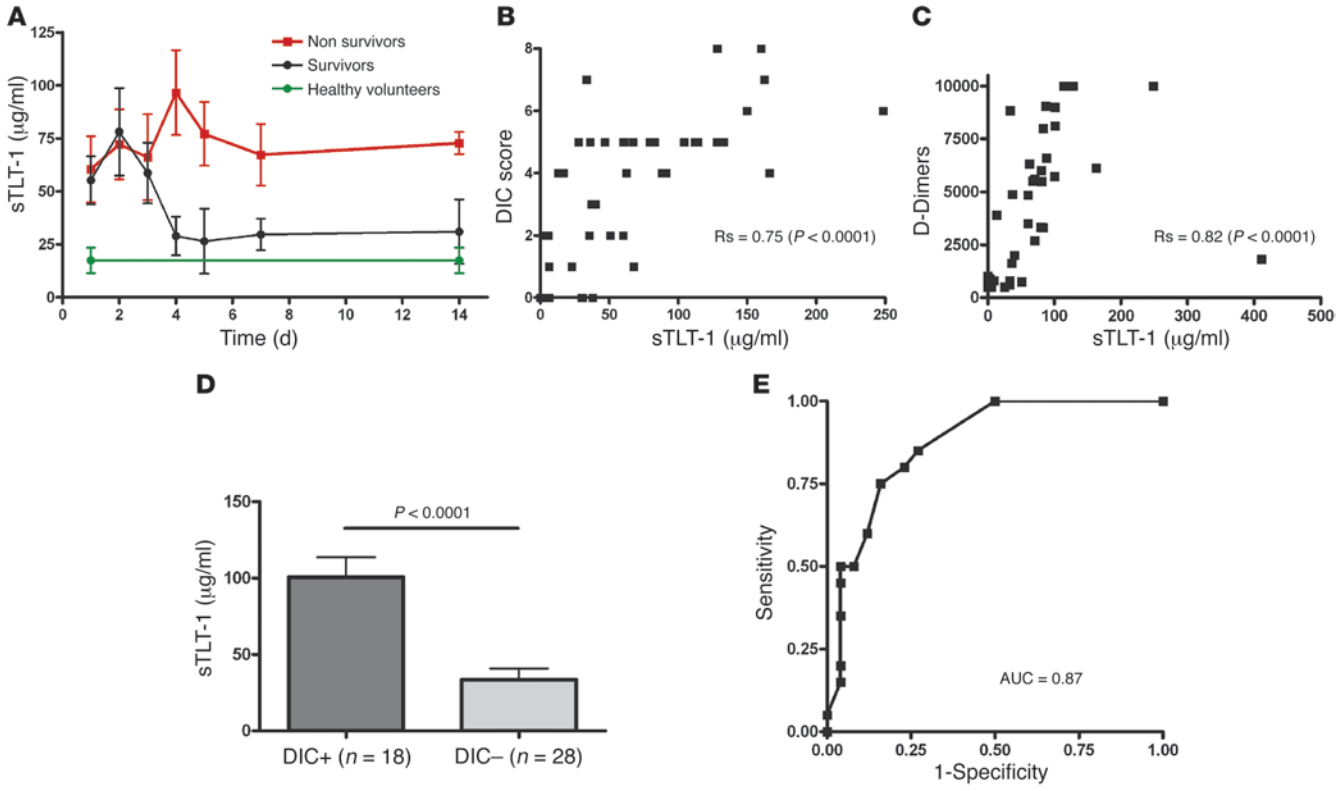

Figure 2
Correlations between sTLT-1, DIC, and outcome in sepsis. (**A**) Time course of plasma sTLT-1 concentrations in surviving (black circles) and nonsurviving patients (red squares). Fifteen healthy donors served as controls (green circles). By day 4, nonsurvivors showed higher sTLT-1 concentrations than survivors ($P < 0.03$, ANOVA). (**B** and **C**) Correlation between plasma sTLT-1 concentration and DIC score as calculated using the ISTH criteria (**B**) or plasma D-dimer levels (**C**). Rs values were calculated via the Spearman test. (**D**) sTLT-1 levels in patients with DIC (DIC score ≥ 5) compared with those without. *P* value represents the results of a Mann-Whitney test. (**E**) ROC curve for sTLT-1 prediction of DIC.

measurement in detecting DIC. To this end, a receiver operating characteristic (ROC) curve was constructed (Figure 2E). Our day 1 sTLT-1 ROC curve showed that at a cut-off set at 50 μg/ml, both the sensitivity and specificity in assessing the presence of DIC were 76%. Taken together, these data suggest that sTLT-1 is strongly associated with septicemia and that sTLT-1 could be an important prognostic indicator for DIC.

Enhancement of platelet aggregation by recombinant sTLT-1. Our previous studies have shown that single-chain anti–TLT-1 antibodies reduce platelet aggregation in vitro, suggesting that, in addition to being an indicator of systemic platelet activation, sTLT-1 might directly modulate platelet aggregation during sepsis (10). To evaluate this possibility, we determined whether recombinant soluble TLT-1 (rsTLT-1) comprised of aa 20–126 might modulate human platelet aggregation, using in vitro aggregation assays (Figure 3). Indeed, addition of rsTLT-1 at concentrations below those found in the plasma of some patients augmented platelet aggregation initiated with 0.5 μM U46619, a TXA_2 mimetic, in a dose-dependant manner (Figure 3A). The specificity of this activity was confirmed by blocking rsTLT-1–enhanced aggregation with a peptide derived from residues 94 to 110 of TLT-1, a region important in TREM-mediated interactions; a control 17-mer peptide had no effect (Figure 3B) (9, 13). Stimulation of platelets with rsTLT-1– or TLT-1–derived peptides alone had no effect (A.V. Washington, unpublished observations). In addition, rsTLT increased platelet aggregation in response to suboptimal concentrations of either ADP (Figure 3C) or collagen (Figure 3D). Interestingly, due to the large disparity in molecular weight between fibrinogen and sTLT-1, the first dose of sTLT-1 with strong effect (60 μg/ml) is roughly equal in molarity to plasma fibrinogen. Thus, sTLT-1 at physiologically relevant concentrations augments platelet aggregation in response to a variety of agonists, suggesting that the sTLT-1 detected in patients may contribute to the hypercoagulative state induced by a systemic inflammatory response.

TLT-1 binds fibrinogen and interacts with ERM family proteins. Our demonstration that antibodies against TLT-1 could inhibit the aggregation of washed platelets suggested that the ligand or ligands for TLT-1 were on or in platelets (10). To gain insight into sTLT-1–mediated increases in aggregation, we sought to identify platelet-derived TLT-1 ligands. Lysates generated from purified human platelets were applied to AminoLink columns preloaded with either sTLT-1 or sTREM-1. After extensive washing, bound proteins were eluted by decreasing pH and multiple fractions were reduced with DTT, resolved with electrophoresis, and visualized by Coomassie staining. This approach revealed specific binding of 3 proteins with molecular masses between 50 and 80 kDa (Figure 4A). Mass spectroscopy identified these proteins as the α, β, and γ chains of fibrinogen (O. Chertov, unpublished data). To confirm these findings, we used histidine-tagged (His-tagged) TLT-1 and TREM-1 bound to nickel columns. After washing and elution of bound proteins with

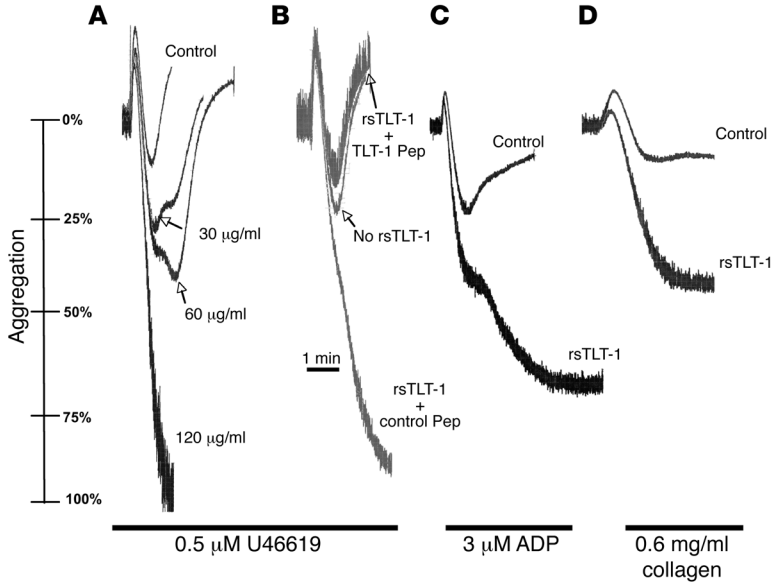

Figure 3
sTLT-1 augments platelet aggregation. Platelet aggregation was initiated by 0.5 μM TXA_2 mimetic, U46610 (**A** and **B**), 3 μM ADP (**C**), or 0.625 μg/ml collagen (**D**) in the presence or absence of the indicated concentration of rsTLT-1 (**A**) or 60 μg/ml (**B**–**D**). In **B**, a peptide (25 μM) composed of a 17-aa stretch (aa 94–110) of TLT-1 or a control peptide was added together with the rsTLT-1. These results are representative of at least 3 experiments.

25% imidazole, aliquots were resolved by PAGE in either native or reduced conditions (Figure 4B). Consistent with disulfide-linked multimers of fibrinogen, our TLT-1 column specifically bound a high molecular weight complex that when reduced resolved into the same 3 bands detected with our AminoLink columns. Immunoblotting with anti-fibrinogen confirmed the identity of these TLT-1–interacting proteins as fibrinogen (Figure 4B).

In order to prove that TLT-1 could bind fibrinogen under more physiologic conditions, we used a chimera, the TLT-1 extracellular domain fused with the Fc domain of human IgG (7). Consistent with TLT-1 interaction with fibrinogen rather than a cell-surface protein, multiple attempts failed to detect binding of this TLT-1–Ig fusion to either activated or resting platelets (A.V. Washington and D.W. McVicar, unpublished observations). However, in ELISA-based experiments, TLT-1–Ig, but not a control Ig-fusion, bound well to plate-bound fibrinogen but not vitronectin (Figure 4C). Collectively, these data establish fibrinogen as a ligand of TLT-1 and suggest that during platelet aggregation, TLT-1 cross-links extracellular fibrinogen, stabilizing higher-order platelet aggregates.

In order to begin to dissect the signaling pathway utilized by TLT-1, we constructed glutathione-*S*-transferase (GST) fusions of its cytoplasmic domain and used them in binding assays using lysates from human platelets. GST–TLT-1, but not GST alone, interacted strongly with a 75-kDa protein from the platelets of 3 independent donors. Mass spectroscopy identified this band as moesin, and immunoblotting confirmed this finding (Figure 5A). Immunofluorescent staining of moesin and TLT-1 confirmed their colocalization, particularly after thrombin stimulation (Figure 5B). Moesin is part of the ERM family of proteins known to link membrane proteins to the actin cytoskeleton. Current reports suggest that of the ERM proteins, only moesin is expressed in human platelets (14). However, because moesin-null mice have no apparent platelet defect (15) and ezrin and radixin are approximately 75% homologous to moesin and thought to have redundant functions (16), we immunoblotted highly purified human and mouse platelets for the presence of all 3 ERMs. Although moesin was most abundant, all 3 proteins were readily detected in mouse platelets and both radixin and moesin were found in human platelets (Figure 5C). Therefore, we addressed the possibility of a TLT-1 interaction with radixin and/or ezrin using a series of reciprocal immunoprecipitations (Figure 5, D and E). TLT-1 coimmunoprecipitated with ezrin in cotransfected HEK293 cells, and endogenous moesin, ezrin and radixin were detected in TLT-1 immunoprecipitations from COS7 cells. Finally, we detected moesin/TLT-1 interactions in primary human platelets (Figure 5F). Collectively, these data suggest that TLT-1 facilitates platelet aggregation by linking fibrinogen to the platelet cytoskeleton via the ERMs.

Defective platelet aggregation and extended bleeding times in mice lacking Treml1$^{-/-}$. In order to better evaluate TLT-1's role in platelet aggregation and inflammation, we deleted exons 1 and 2 of *Treml1* (the gene encoding TLT-1) in C57BL/6 mice. Homozygous *Treml1*$^{-/-}$ mice were identified by PCR using a 3-primer system, and identification was confirmed by Southern blot analysis (Figure 6, A–C). Null mice were viable, fertile, and completely devoid of TLT-1 protein, as demonstrated using antibodies to either the extracellular or intracellular (A.V. Washington, unpublished observations) regions of the receptor by Western blot and confocal analysis (Figure 6, D and E). Although *Treml1*$^{-/-}$ mice had somewhat higher leukocyte counts (13.98 ± 0.9 vs. 11.88 ± 1.1, $n = 7$) and slightly lower platelet counts than WT mice (761.0 ± 44.5 vs. 949.6 ± 35.69, $n = 7$; $P = 0.006$), only the platelet differences reached statistical significance.

Our previous in vitro studies have shown that single-chain anti–TLT-1 antibodies reduce platelet aggregation (10), whereas here we show that recombinant sTLT-1 facilitates aggregation (Figure 3). Therefore we tested *Treml1*$^{-/-}$ platelet aggregation using thrombin, collagen, ADP, or the TXA_2 mimetic U46619. Regardless of the agonist, *Treml1*-null platelets were able to commence normal shape change, as indicated by the transient decrease in light transmission (Figure 7, A–D). However, *Treml1*$^{-/-}$ platelets reproducibly aggregated less efficiently when stimulated with thrombin (Figure 7A) or collagen (Figure 7B). Defects in *Treml1*$^{-/-}$ platelet aggregation were even more pronounced when ADP (Figure 7C) or U46619 (Figure 7D) were used as agonists. In accordance with our identification of fibrinogen as a TLT-1 ligand, *Treml1*$^{-/-}$ platelets bound demonstrably lower amounts of fibrinogen as compared with their WT counterparts (Figure 7E). Notably, with all 4 agonists, distinct aggregation defects were evident at all concentrations tested (A.V. Washington, unpublished observations), suggesting that TLT-1 plays a fundamental role in platelet aggregation. Finally, to evaluate the potential effects of the TLT-1 aggregation defect in vivo, we compared bleeding times between *Treml1*$^{-/-}$ and WT mice. Bleeding times in the null mice were double that of controls (87.33 ± 13.73 seconds [controls] vs. 184.33 ± 57.57 seconds [*Treml1*$^{-/-}$]; $n = 12$; $P = 0.05$), consistent with the decreased, but not absent, ability of *Treml1*$^{-/-}$ platelets to aggregate in vitro (Figure 7F).

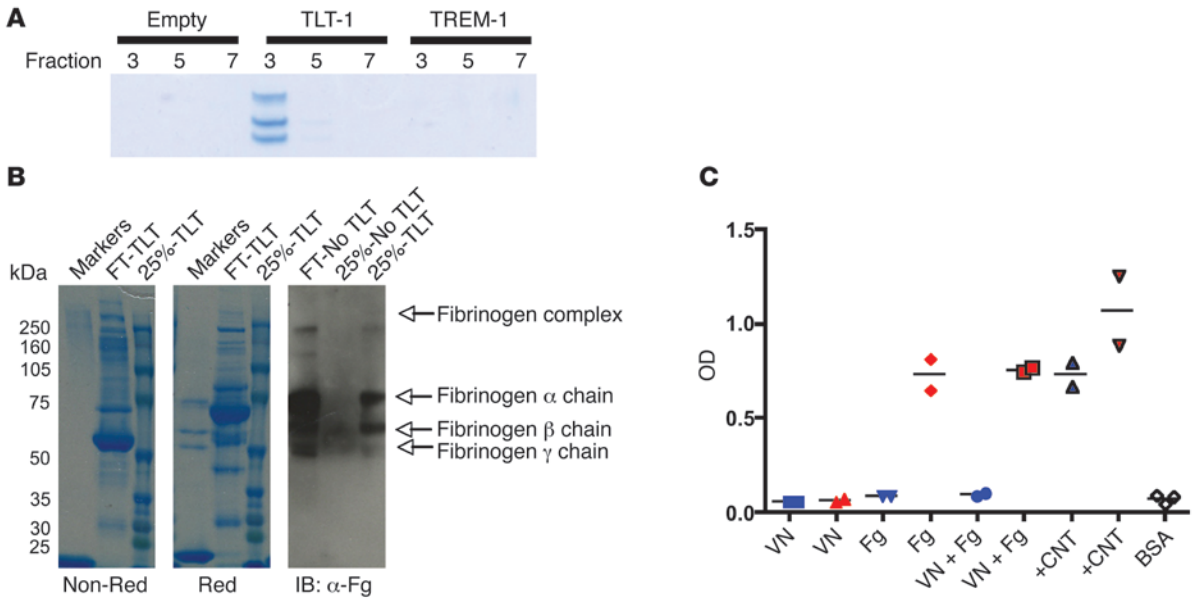

Figure 4

Fibrinogen interaction with TLT-1. (**A**) Elution fractions from an unloaded AminoLink column (empty) and columns loaded with TLT-1 and TREM-1 after exposure to platelet lysate, washing, and elution with decreasing pH. Fractions 3, 5, and 7 from each column were resolved by PAGE and were stained with Coomassie blue. (**B**) Fractions eluted off nickel column preloaded with purified TLT146-His or TREM-1–His (no TLT) and exposed to platelet lysate. Flow-through (FT) and proteins eluted by 250 mM imidazole (25%) were resolved by PAGE in nonreduced (nonred, left panel) or reduced form (red, 2 right panels). Gels were stained with Coomassie blue (left 2 panels) or immunoblotted with anti-fibrinogen (IB: α-Fg, right panel). (**C**) TLT-1–Ig (red) or control Ig fusion (blue) binding to plate-bound vitronectin (VN), fibrinogen (Fg), or BSA. Positive controls (+CNT) were Ig fusions bound directly to plastic. After washing, bound Ig fusion was detected using anti-human Ig. Markers represent individual determinations, and the horizontal lines represent the mean.

TLT-1 regulates the systemic response to LPS. The elevated levels of sTLT-1 in septic patients and the role of TLT-1 in platelet function prompted us to assess the effects of LPS administration on WT and *Treml1*$^{-/-}$ mice. Consistent with our findings in septic patients, i.p. LPS administration led to detectable levels of sTLT-1 within 2 hours that continued to climb throughout the 24-hour study (Figure 8A). To assess whether sTLT-1 levels might correlate with other parameters of endotoxemia, we measured TNF, platelet counts, leukocyte numbers, and D-dimer levels in these mice. As expected, administration of LPS resulted in the production of TNF, severe thrombocytopenia, and leukocytopenia over the study period (Figure 8, B–D). TNF production peaked 2 hours after LPS exposure and matched the leukocyte nadir. In contrast, platelet counts fell by about 30% within the first 2 hours, then steadily decreased further thereafter (Figure 8C). Importantly, the pattern of thrombocytopenia closely mirrored the increase in sTLT-1 (r^2 = -0.922), suggesting sTLT-1 is released or shed as platelets leave the circulation during endotoxemia. Under these conditions, D-dimers were not detected in the blood of WT mice until 24 hours after LPS injection (A.V. Washington, unpublished observations). Therefore, sTLT-1 is associated with the septic response in mice, in which it is inversely correlated to platelet count but readily detectable well before clinically relevant thrombocytopenia. Given the dramatic variability in platelet number across the human population and the lack of detectable D-dimers until endotoxemia is well established, these data suggest that sTLT-1 levels may represent a more powerful prognostic indicator of developing DIC than these commonly used parameters.

When challenged with LPS, *Treml1*$^{-/-}$ mice exhibited signs of endotoxemia that included hunching and the appearance of a rough coat similar to that of WT mice. We next assessed LPS-induced thrombocytopenia, leukocytopenia, TNF, and D-dimers in *Treml1*$^{-/-}$ mice. Although LPS-induced leukocytopenia (WT: 5.296 ± 1.13 × 10^3/ml; *Treml1*$^{-/-}$: 5.211 ± 0.59 × 10^3/ml, n = 9; P = 0.948) and thrombocytopenia (WT: 451.4 ± 75.67 × 10^6/ml; *Treml1*$^{-/-}$: 319.7 ± 39.9 × 10^6/ml, n = 9; P = 0.143) were unaffected in the null mice, we found increased TNF and D-dimers in *Treml1*$^{-/-}$ mice relative to controls (Figure 9, A and B). From our studies, we cannot conclusively determine whether the increased levels of D-dimer in *Treml1*$^{-/-}$ mice is due to increased coagulation or decreased fibrinolysis; however, consistent with the increased production of TNF and increased D-dimer production following LPS injection, *Treml1*$^{-/-}$ mice died faster than WT, with a median survival time of 40 hours as compared with 48 hours (log-rank test; P = 0.049) (Figure 9C). In addition, whereas in this and multiple smaller experiments, 15%–20% of WT mice survived LPS challenge, all the *Treml1*$^{-/-}$ mice routinely succumbed. Taken together, these data suggest that TLT-1 provides benefit to the host during endotoxemia, perhaps by limiting TNF production.

Increased inflammatory hemorrhage in Treml1$^{-/-}$ *mice*. Having established a role for TLT-1 in platelet function and demonstrated its association with sepsis, we evaluated the role of TLT-1 in controlling hemorrhage associated with vascular injury secondary to inflammation. To this end, we employed the localized Shwartzman model of hemorrhagic vasculitis. The localized Shwartzman reaction is a surrogate of the septic response and DIC in humans, producing a local lesion amenable to direct evaluation (17). Consistent with the ability of TLT-1 to help maintain vascular integrity, the hemorrhagic Shwartzman lesions of

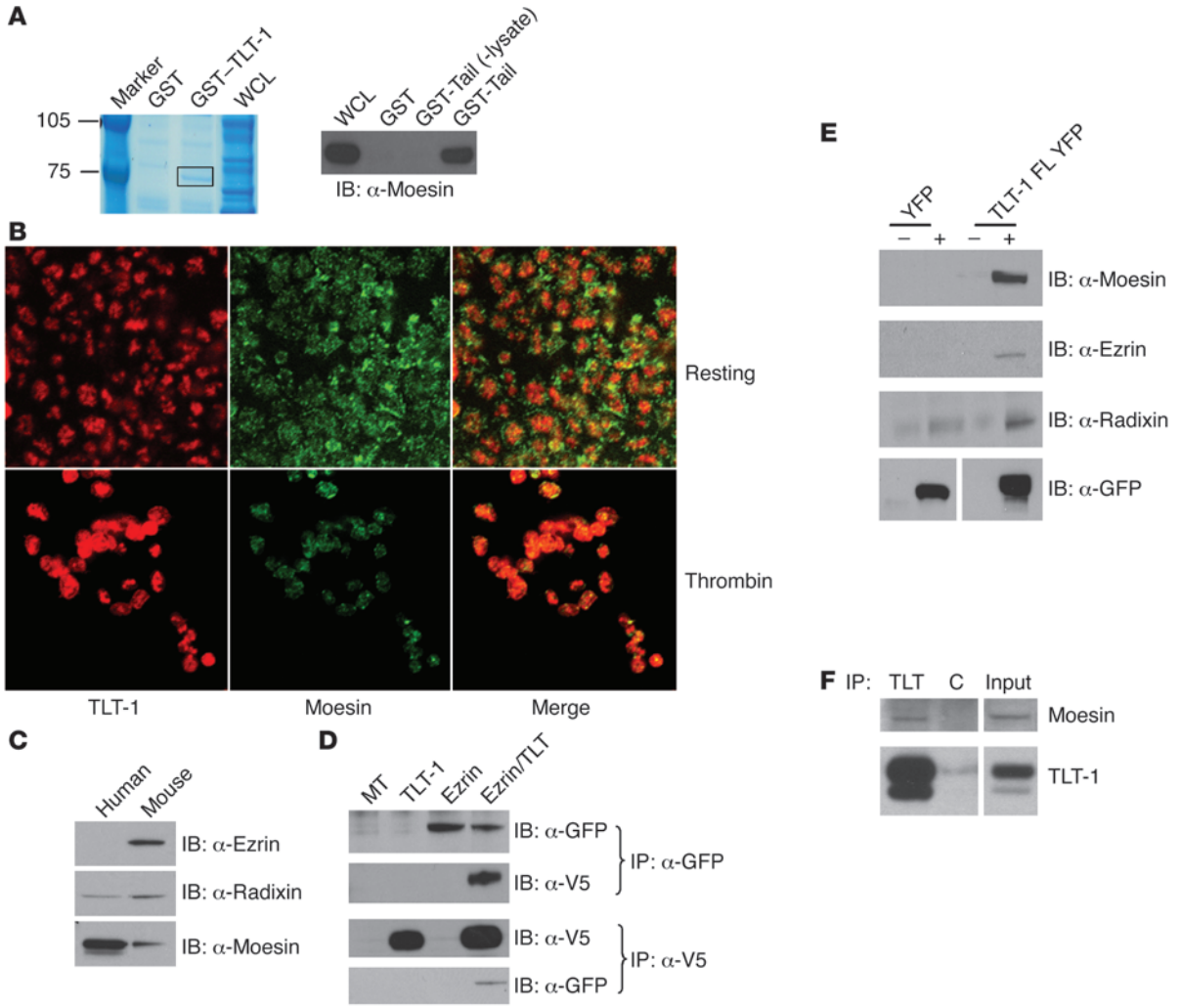

Figure 5

The cytoplasmic tail of TLT-1 binds ERMs. (**A**, left panel) Whole-cell lysate (WCL) or proteins bound to GST alone or GST–TLT-1 cytoplasmic tail (GST–TLT-1) were stained with Simply Blue (Invitrogen). The unique TLT-1–binding protein is boxed. (**A**, right) Proteins as above were immunoblotted with anti-moesin. Elutes of GST–TLT-1 that were not exposed to platelet lysate are in lane 3. (**B**) Confocal fluorescent images of resting platelets (top panels) and those activated for 2 minutes with thrombin (bottom panels). Cells were stained with goat anti–TLT-1 (red) and rabbit anti-moesin (green). Original magnification, ×633. (**C**) Whole-cell lysates from highly purified human (lane 1) or mouse (lane 2) platelets were probed with ERM antibodies as indicated. (**D**) HEK293 cells were mock transfected (MT) or cotransfected with V5-tagged TLT-1 and/or GFP-tagged ezrin as indicated. Lysates were immunoprecipitated and probed as indicated. (**E**) Cos7 cells transfected (+) or not (–) with either yellow fluorescent protein (YFP) alone or a TLT-1 YFP construct were immunoprecipitated with anti-YFP and probed as indicated. (**F**) Primary human platelets were either stimulated (+) or not (–) with thrombin, then lysed, and TLT-1 was immunoprecipitated with anti–TLT-1 or control (C) antibody. Filters were probed with anti-moesin, then anti–TLT-1.

Treml1$^{-/-}$ mice were almost 4 times the size of those in WT mice (Figure 10A). Microscopic evaluation of these lesions supported these macroscopic observations (Figure 10B). Using a grading system of 1 to 4 (see Methods), we compared the lesions from mice of each genotype for microclots, thrombi, lesion size, hemorrhage, and neutrophil influx. Overall, *Treml1*$^{-/-}$ mice exhibited fewer occlusive thrombi, more microclots, and increased neutrophil influx relative to WT, although these differences were not significant (A.V. Washington, unpublished observations). In contrast, there was nearly twice the degree of microscopic hemorrhage associated with the Shwartzman lesions of *Treml1*$^{-/-}$ mice compared with those of WT mice (Figure 10, C and D). These results dramatically demonstrate that TLT-1 is critical in controlling hemorrhage associated with the inflammatory response.

Discussion

Our previous work has suggested that the TLT-1 extracellular domain is shed from platelets during activation (9). The potential biological significance of the sTLT-1 fragment is reinforced by the existence of 2 splice variants with limited or absent intracellular domains. The first is the most abundant TLT-1 mRNA species and possesses an extracellular domain identical to that of full-length TLT-1 but only a 16-aa cytoplasmic domain (18). The second

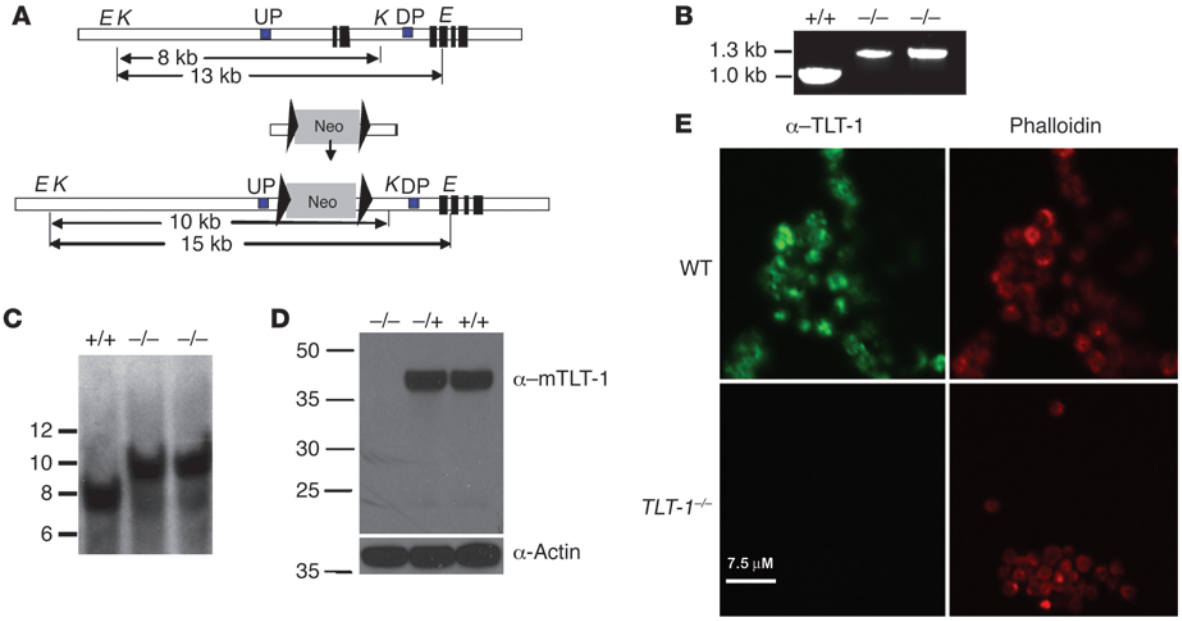

Figure 6
Targeting of the *Treml1* locus. (**A**) A schematic representation of the *Treml1* genomic region and the strategy for replacement of exons (black boxes) 1 and 2 with the Neo cassette (gray rectangle). The positions of restriction sites for EcoRI (E) and KpnI (K) are noted as are the positions of the upstream (UP) and downstream (DP) probes used for Southern blot analysis of recombinants. (**B**) PCR analysis of tail DNA from 1 WT and 2 *Treml1*-null mice. Primers 1 and 2 amplify products of 947 bp (WT), and primers 1 and 3 amplify a product of 1250 bp (null). (**C**) Southern analysis of tail DNA from 1 WT and 2 homozygote null mice digested with KpnI and probed with UP. (**D**) Western blot of whole-cell extracts of platelets from *Treml1*$^{-/-}$, WT, or heterozygote mice (top). Immunoblotting for actin served as a loading control (bottom). (**E**) Confocal analysis of U46619-activated WT and null platelets stained with anti–TLT-1 antibody (left panels) or phalloidin (right panels). Scale bar: 7.5 μM.

form was recently identified in our laboratory and encodes only the TLT-1 extracellular domain (A.V. Washington, unpublished observations). From an evolutionary perspective, the presence of these truncated and soluble species in both mice and humans argues for an important role for the extracellular domain in physiology. Therefore, here we addressed the possibility that sTLT-1 might be released under pathological conditions, resulting in changes in platelet function during those disease states. Based on this paradigm, we hypothesized that during rife, unfocused platelet activation associated with sepsis (11), we might detect abnormally high levels of sTLT-1.

Data from 2 independent cohorts confirmed the presence of increased levels of sTLT-1 in sepsis patients. Our initial study incorporated patients in the very early stages of sepsis, as indicated by their relatively low SOFA scores, as compared with our in-depth study. Our original patients also had much higher levels of sTLT than the cohort, with higher SOFA scores suggesting that sTLT-1 may spike early in the septic response. However, clinical characteristics of some patients in our initial study, including HIV infection, limit these interpretations. Our finding that patients who died during sepsis had increasing levels of sTLT-1 in the 2 days following admission to the ICU, whereas those who survived showed declines in sTLT-1 during this same period, suggest that monitoring of sTLT-1 levels could be an important prognostic indicator. Similarly, the correlation between sTLT-1 and D-dimers indicates association of sTLT-1 with the clinical manifestations of DIC. In support of this conclusion, ROC curve analysis showed that at 50 μg/ml, sTLT-1 has good sensitivity and specificity as an indicator for DIC. In fact, a recent report found that 3 criteria included in the current ISTH classification of DIC (platelet count, AUC 0.67; prothrombin time, AUC 0.74; and fibrinogen AUC, 0.70) all had AUC values below what we find for sTLT-1 as an indicator of DIC (19). Taken together, these data clearly demonstrate the involvement of TLT-1 in the host response to sepsis and indicate that sTLT-1 may provide a significant clinical tool for the diagnosis of DIC associated with sepsis, perhaps becoming readily detectable well before other manifestations of DIC.

The ability of anti–TLT-1 scFv to block aggregation of washed platelets suggested that TLT-1 facilitates thrombosis by interacting with a ligand or ligands on or in activated platelets (10). Our finding here that clinically relevant levels of sTLT-1 directly promote platelet aggregation in vitro suggests that TLT-1 may be a novel, platelet-specific, secondary activation factor, poised to promote aggregation in situations where only low levels of agonist are present yet vascular integrity must be maintained. This conclusion is bolstered by our demonstration of significant platelet aggregation defects and extended bleeding times in *Treml1*$^{-/-}$ mice. Surprisingly, we even detected aggregation defects in *Treml1*$^{-/-}$ platelets stimulated with ADP, an agonist not normally associated with the release of α-granules. However, our analysis of TLT-1 expression in whole blood isolated from human donors or mice confirmed the ability of ADP to induce TLT-1 expression on platelets, this despite the recent confirmation of TLT-1's location within α-granules via ultrastructural analysis (20). Oddly enough, our flow cytometrical analysis of sTLT-1–mediated amplification of platelet aggregation failed to demonstrate any direct binding of sTLT-1 to resting or activated platelets (A.V. Washington, unpublished observations). Instead, we found that TLT-1 binds fibrinogen. These data

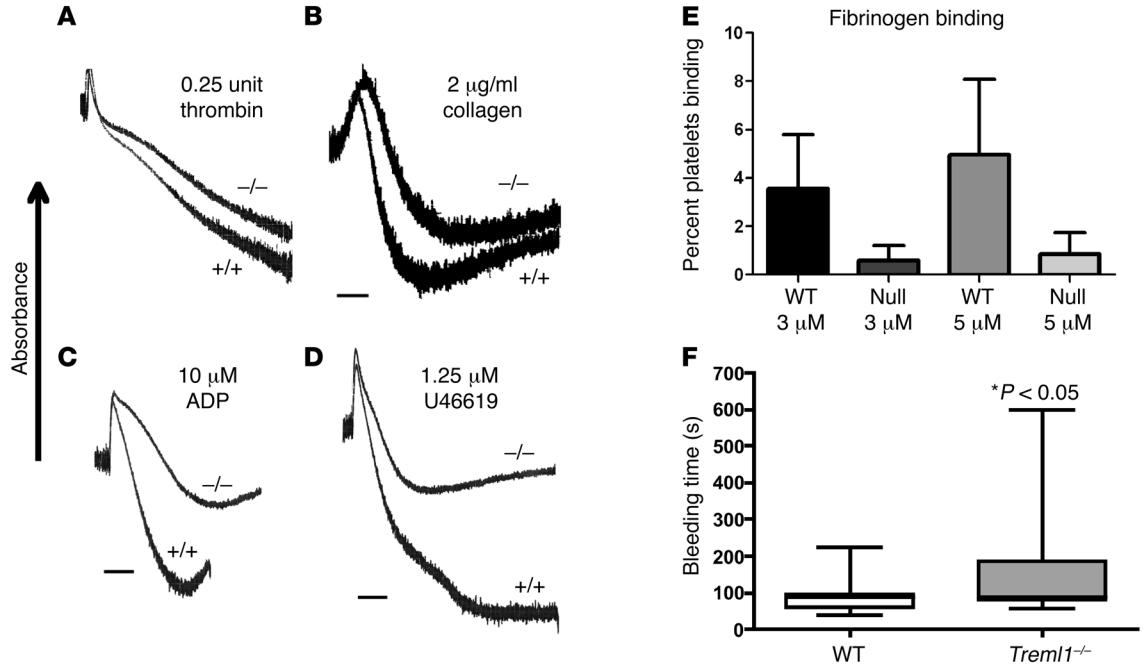

Figure 7

Platelet aggregation defects and extended bleeding times in *Treml1*$^{-/-}$ mice. (**A**–**D**) Platelet-rich plasma from WT or *Treml1*$^{-/-}$ mice was isolated from citrated blood, and aggregation was measured using thrombin (**A**), collagen (**B**), ADP (**C**), or U46619 (**D**) as agonists. These results are representative of at least 3 experiments. (**E**) Percentage of platelets activated with suboptimal doses of ADP that bind fibrinogen, as determined in whole-blood flow cytometry analysis. (**F**) Bleeding time measured by tail snip assay in WT and *Treml1*$^{-/-}$ mice. Lower boundary of the whisker box is the 25th percentile, and the upper boundary is the 75th percentile. The line within the box is the median, and the whiskers represent the highest and lowest values. $n = 12$ for each group; $P < 0.05$ by Student's t test.

are consistent with a model in which, during platelet activation, stored fibrinogen is secreted and cross-linked by both sTLT-1 and cell surface TLT-1. The inability of TLT-1 to interact with vitronectin or fibronectin suggests that unlike GPIIb/IIIa, TLT-1 likely does not interact with RGD-type sequences found in fibrinogen, a conclusion not unexpected given the distinct structural properties of integrins and TREM (9). Rather, the use of unique binding sites suggests that TLT-1 may work in concert with GPIIb/IIIa to facilitate fibrinogen/platelet interactions and/or higher-order platelet aggregation. Future detailed biochemical analysis of the TLT-1/fibrinogen interaction will clarify these possibilities.

Our biochemical analysis also showed that the TLT-1 cytoplasmic tail interacts strongly with the ERM protein moesin. Thus, TLT-1 becomes the second ITIM-containing receptor in platelets shown to interact with the ERMs, PECAM being the other (21). Although others have suggested that moesin is the only ERM in mouse platelets, moesin-null mice don't show an aggregation defect as *Treml1*$^{-/-}$ mice do (15). We could readily detect ezrin and radixin in purified mouse platelets and found that both these proteins also interact with TLT-1, leading us to conclude that in the absence of moesin, TLT-1 couples to other members of the ERM family. The ERMs are implicated in the formation of filopodia and lamellipodia in various cell types, including platelets. Moesin signaling is regulated downstream of Rho by phosphorylation at Thr558 in a process controlled by myosin phosphatase and Rho kinase, both of which play a role in platelet activation during shape change (15, 22–24). Thus, the interaction of TLT-1 with moesin we report here is consistent with our previous scFv studies that suggested that TLT-1 functions after shape change (10). Moreover, when we assessed CD62 expression by flow cytometry, we found no differences between *Treml1*$^{-/-}$ and WT platelets, suggesting that initial agonist signaling is not affected by the lack of TLT-1 (A.V. Washington, unpublished observations). Collectively, these findings support a model in which platelet activation causes TLT-1 to be brought to the platelet surface, facilitating the release of sTLT-1. After shape change and degranulation, TLT-1 binds fibrinogen and guides rapid pseudopodia formation in platelets though interaction with moesin and other ERM proteins, resulting in enhanced higher-order platelet aggregation. This model places TLT-1 in an emerging class of platelet regulatory molecules, including CD40L (25), Gas6 (26), CD36 (27), and the eph kinases (28), that assist thrombin, fibrinogen, and collagen with control of the more subtle aspects of platelet aggregation, providing a critical mechanism allowing for hemostasis without thrombosis.

Our establishment of a direct role for TLT-1 in the regulation of platelet aggregation together with the elevated sTLT-1 levels in septic patients and its association with DIC raised the possibility that the release of sTLT-1 during sepsis may be beneficial in maximizing platelet aggregation at sites of vascular damage during the inflammatory response. Alternatively, by virtue of their ability to reduce the aggregation threshold in the periphery, the high systemic levels of sTLT-1 detected in patients might contribute to aberrant platelet aggregation at distal sites, potentiating the development of DIC and the subsequent depletion of coagulation factors that contribute to morbidity (1, 11). When we assessed TLT-1 during endotoxemia in mice, we found detectable levels of sTLT-1 within 2 hours

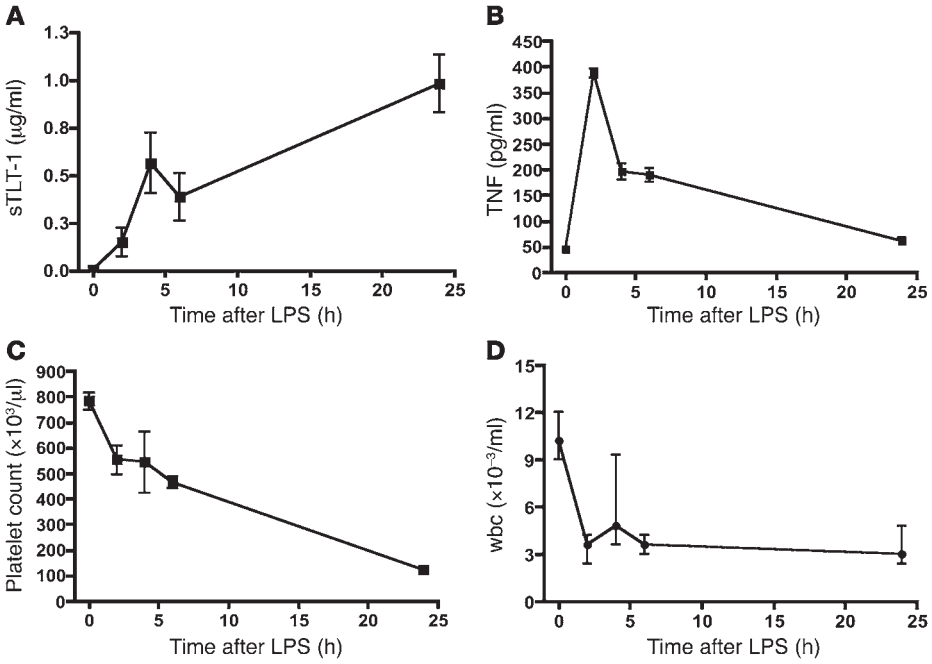

Figure 8
Relationships among sTLT-1, TNF, platelet, and leukocytes counts during endotoxemia. Blood from naive C57BL/6 mice (T0) or mice injected i.p. with LPS (5 mg/kg) was collected at the indicated times after LPS. Plasma sTLT-1 (**A**) and TNF (**B**) levels were assessed by dot blot or ELISA analysis, respectively. Platelet (**C**) and leukocyte (**D**) counts were derived from whole-blood analysis. Results of **A**, **B**, and **C** represent the mean ± SEM. Data in **D** indicate median ± IQR.

of LPS administration. The levels of sTLT-1 were in strong inverse correlation with platelet counts. Moreover, in these experiments, we did not detect an increase in cell surface TLT-1 on platelets remaining in the circulation, and when stimulated ex vivo, these platelets expressed normal levels of TLT-1 (D.W. McVicar and A.V. Washington, unpublished observations). Therefore, sTLT-1 is most likely released only by platelets as they leave the circulation during endotoxemia, not from the remaining circulating pool.

In normal mice, LPS causes a spike in TNF levels 2 hours after injection; these levels fall as sTLT-1 levels increase. This relationship opens the possibility of a direct feedback mechanism involving sTLT-1 and TNF-producing cells. Indeed, activated platelets have been reported to express a TREM-1 ligand, interact with neutrophils and monocytes, and enhance neutrophil response to LPS via TREM-1 (29). Although these initial reports suggested TLT-1 is not itself the TREM-1 ligand on activated platelets, we cannot currently rule out inhibition of these platelet leukocyte interactions as the mechanism whereby TLT-1 tempers inflammation (29).

Our challenge of *Treml1*$^{-/-}$ mice with LPS confirmed a role for TLT-1 in both the inflammatory and consumptive phases of sepsis. Although LPS-induced leukocytopenia was largely unaffected in *Treml1*$^{-/-}$ mice, these mice had higher serum levels of TNF and higher levels of D-dimers following LPS than did WT mice. However, these changes translated into only a limited survival benefit for the *Treml1*$^{-/-}$ mice, likely because DIC does not play a significant role in the mortality associated with endotoxemia in mice (30). Thus, we propose that TLT-1 primarily supports platelet aggregation at sites of inflammatory vascular injury, thereby controlling vascular integrity during the septic response. This interpretation is strongly supported by the results of our analysis of localized Shwartzman reactions in *Treml1*$^{-/-}$ mice. Although not all models of inflammation-induced hemorrhage are dependent on platelet adhesion, the Shwartzman reaction is, as indicated by exacerbated hemorrhage in P selectin–null mice (2, 31). Accordingly, we found that removal of TLT-1 slightly increased neutrophil influx at the site of injection and that Shwartzman lesions were demonstrably more hemorrhagic in *Treml1*$^{-/-}$ mice. Thus, our data suggest that TLT-1 may minimize vessel damage by regulating the production of TNF and augment platelet aggregation at the site of vessel injury, preventing hemorrhage. Therefore, we suggest that the high levels of sTLT-1 detected in patients who die from sepsis likely indicate the hemostatic system's aggressive attempts at maintaining vascular integrity as well as efforts by the host to contain the inflammatory response.

In summary, our data establish TLT-1 as a molecule capable of fine-tuning platelet aggregation and inflammation for the control of vascular integrity. As such, its characterization has revealed a unique opportunity for the therapeutic separation of the benefits of hemostasis from the detriment of thrombosis. Based on our findings, we predict that specific intervention with TLT-1 or TLT-1–mediated signals might have potential in the therapy of a variety of hypercoagulatory states, including those associated with sepsis.

Methods

Initial study population. The Universidad Central del Caribe Escuela del Medicina Institutional Review Board (Federalwide Assurance no. FWA00001103) approved the study, and patients or their surrogates provided written informed consent before enrollment (protocol no. 200619; primary investigator, I. Acevedo). All patients 18 years of age or older who were hospitalized and diagnosed with sepsis during a 1-month period were invited to participate in the study. Sepsis and its stages were judged according to the established consensus. The following were recorded for each patient on admission into the ICU: age; sex; severity of underlying medical condition stratified according to the criteria of SAPSII (32) (Acute Physiology, Age, Chronic Health Evaluation II [APACHE II]: scores can range from 0 to 71, with higher scores indicating a higher risk of death); SOFA (33) score (the total score can range from 0 to 24, with scores for each organ system [respiration, coagulation, liver, cardiovascular, central nervous system, and kidney] ranging from 0 [normal] to 4 [most abnormal]); and the reason for admission to the ICU. The following baseline variables were also

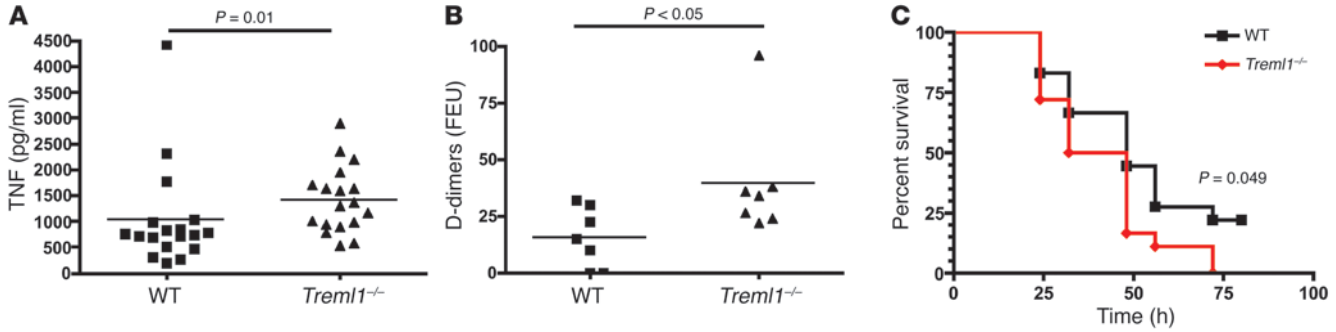

Figure 9

Accentuated TNF, thrombocytopenia, D-dimer production, and decreased survival in LPS-treated *Treml1*$^{-/-}$ mice. (**A**) WT and *Treml1*$^{-/-}$ mice ($n = 18$) were challenged i.p. with 6 mg/kg LPS. After 2 hours, blood was collected from the retroorbital plexus and serum TNF was assayed. Markers represent individual animals, and horizontal lines represent the mean. $P = 0.01$ by Mann-Whitney test. Survival was then monitored over the next 80 hours (**C**). $P < 0.05$ by log-rank test. (**B**) Mice of the indicated genotype were injected i.p. with LPS. Twenty-four hours later, plasma levels of D-dimer were determined. Markers represent individual animals, and horizontal lines represent the mean. $P < 0.05$ by Student's *t* test.

recorded at enrollment: body temperature; leukocyte count; and ratio of the partial pressure of arterial oxygen to the fraction of inspired oxygen (PaO_2:FiO_2). The length and the outcome (death or discharge) of stay in the ICU were also recorded. D-dimers were measured by ELISA according to manufacturer's specifications (Aniara).

Longitudinal study patient population. Between July and December 2007, all consecutive patients with septic shock admitted into a 16-bed medical intensive care unit of Hôpital Central were enrolled. Data for this study were derived from pathological waste samples, and the NIH Office of Human Subjects Research reviewed and approved inclusion of data from this study (approval no. 4037). Approval of the institutional review board and informed consent was obtained from patients or their relatives before inclusion.

The diagnosis of septic shock was established on the basis of current definitions. Patients were not enrolled if they were more than 80 years of age or were immunocompromised (treatment with corticosteroids >1 mg/kg equivalent prednisone; bone marrow or organ transplant recipients; neutropenia [neutrophil count < 0.5×10^9/l]; hematologic malignancy; or AIDS). Upon admission into the ICU, age, sexual phenotype, severity of underlying medical condition stratified according to the criteria of McCabe and Jackson (34), SAPSII (35), SOFA score (33), vital signs, respiratory variables, routine blood test results, and microbial culture results were recorded. The DIC score was calculated according to ISTH recommendations (12). Outcome was assessed during a 28-day follow-up period.

Dot blot analysis. Levels of sTLT-1 in samples of patient plasma were measured by immunoblot technique using a goat polyclonal antibody against human TLT-1 (R&D Systems). Patients' samples were subjected to a series of dilutions (1:3), and 100 μl of each dilution was dotted onto a nitrocellulose membrane, dried, and subjected to 5% milk blocking for 1 hour. The nitrocellulose sheet was then incubated for 60 minutes in the presence of antibody (dilution, 1:1000). After thorough washing, the sheet was incubated for another 60 minutes with rabbit anti-goat antibody (dilution, 1:10,000; Pierce, Thermo Scientific) in 5% milk block washed 3 additional times with Tris-buffered saline with 0.1% Tween-20 and visualized with substrate (Pierce, Thermo Scientific). Each sheet also contained calibration samples of a known concentration of rsTLT-1 (0 to 10 μg/ml). Densitometric determination was achieved by means of the VersaDoc and Quantity One Quantitation Software, version 4.6.3 (Bio-Rad). The level of sTLT-1 in each sample was determined by comparing the OD of the samples with that of the standard curve. All measurements were performed in duplicate, and the results are expressed as μg/ml plasma.

Nickel and AminoLink affinity columns. We used AminoLink Plus Coupling Resin Kit (Pierce, Thermo Scientific). TLT107 or TREM-1 was coupled to the column according to manufacturers' specifications, and platelet lysate was applied and washed until UV absorbance returned to baseline. Bound proteins were eluted according to manufacturers' specifications. Three nickel-chelating column runs were performed, the first with a column preloaded with purified TLT146-His. After preloading the column, platelet lysate was passed over the column and flow-through was collected. The column was washed as above, then with 20 mM imidazole, and finally with 50 mM imidazole. TLT-1 and bound proteins were then eluted with 250 mM (25%) imidazole. This same process was repeated, preloading the column with TREM-1–His or without preloading the column as controls.

TLT-1–Ig binding to fibrinogen. One-hundred microliters of protein solution was incubated in 96-well Nunc-Immuno Plates with MaxiSorp surface (Nalgen) for either 2 hours at 37°C or overnight at 4°C. Plates were washed 2 times with PBS, blocked with 1% BSA for 30 minutes at room temperature, and washed 2 times with PBS/0.5% Tween-20; the chimeric protein (50 ng/ml) was added for 1 hour. Plates were washed 3 times with PBS/0.5% Tween-20 and incubated with goat anti-human HRP secondary antibody (Jackson ImmunoResearch Laboratories Inc.) for 30 minutes, washed 4 times with PBS/0.5% Tween-20 and 1 time with PBS, and then developed using 100 μl TMB substrate (SureBlue; KPL). The reaction was stopped using KPL Stop Solution, and the plates were read at 452 nM.

Confocal analysis. Platelets were prepared as described in ref. 7. Confocal analysis was completed on an Olympus FV1000 SIM Scanner inverted microscope system equipped with a ×60/1.43 oil objective (Olympus). Images were analyzed using Olympus FluoView software, version 1.7b.

Mice. *Treml1*$^{-/-}$ and control C57BL/6 mice of the same sexual phenotype and age were maintained under specific pathogen–free conditions at the National Cancer Institute and at the Universidad Central del Caribe animal facility. Animal care was provided in accordance with the procedures outlined in *Guide for the care and use of laboratory animals* (NIH publication no. 85-23. Revised 1985). All mice were between 18 and 30 g. Ethical approval for the animal experimentation detailed in this article was received from the Institutional Animal Care and Use Committee at the National Cancer Institute (Office of Laboratory Animal Welfare assurance no. A4159-01) and/or Animal Welfare Assurance/Universidad Central del Caribe Institutional Universidad Central del Caribe School of Medicine (OLAW assurance no. A3566-1).

Whole-blood flow cytometry. Aliquots of murine blood (5 μl) were added to microcentrifuge tubes containing HEPES–Tyrode's buffer (5 mM HEPES,

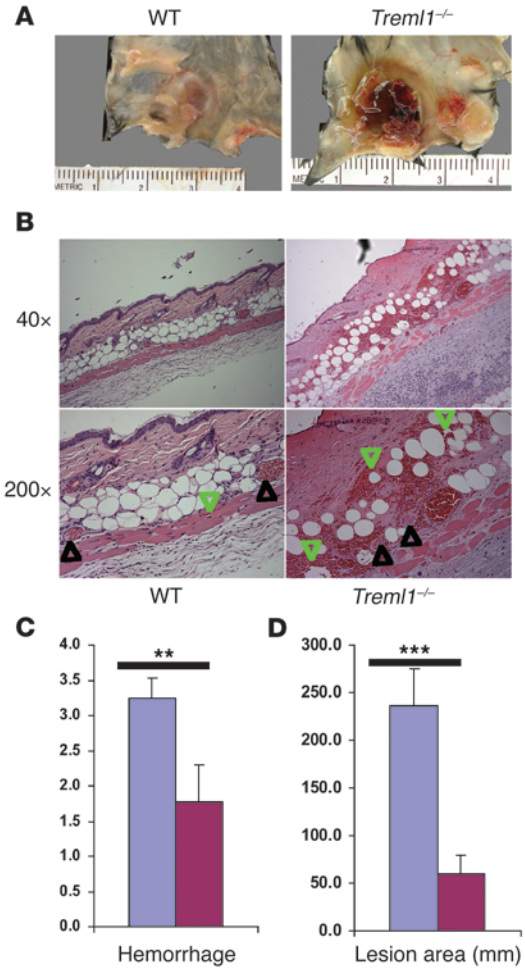

Figure 10
Targeted deletion of *Treml1*$^{-/-}$ results in increased hemorrhage associated with inflammation. (**A**) Representative macroscopic views of Shwartzman lesions from WT and *Treml1*$^{-/-}$ mice. (**B**) Microscopic view of Shwartzman lesions of WT and *Treml1*$^{-/-}$ mice. Skin sections from WT and *Treml1*$^{-/-}$ mice are shown stained with H&E. Areas of hemorrhage are marked with green arrowheads. Characteristic thrombi are marked by black arrowheads. Original magnification, ×40 (top panels); ×200 (bottom panels). (**C** and **D**) The lesions of the Shwartzman reaction were scored for hemorrhage as defined in Methods (**C**) and area of the lesion (**D**). WT, maroon, $n = 9$; *Treml1*$^{-/-}$, blue, $n = 8$. $^{**}P < 0.05$; $^{***}P < 0.001$ by Student's t test. Error bars indicate SD.

137 mM NaCl, 2.7 mM $NaHCO_3$, 0.36 mM NaH_2PO_4, 2 mM $CaCl_2$, 4 mM $MgCl_2$, and 5 mM glucose, pH 7.4) and fluorochrome-labeled ligands (all from BD Biosciences). For assessment of platelet function, the microcentrifuge tubes contained either no platelet agonist (for assessment of baseline activation) or ADP (3 μM or 5 μM) to activate platelets. A PE-conjugated antibody against GPIIb (CD41; BD Biosciences) was used as an activation-independent marker of platelets. Alexa Fluor 594–conjugated fibrinogen (Invitrogen) was added to permit assessment of fibrinogen binding. A FITC-conjugated antibody against CD62 was used to delineate platelet surface expression of P selectin. The reaction mixture (total volume of 65 μl) was incubated for 15 minutes at room temperature. Subsequently, FACS Lysing Solution (BD Biosciences) was added to fix the platelets and lyse erythrocytes. All assays were performed in triplicate and results reported as the averages of the 2 determinations. Flow cytometric analysis was performed with the use of a FACS Scan (BD). For analysis of platelet function, platelets were identified on the basis of size and binding of anti-CD41. To assess nonactivation-dependent protein association with platelets, PE-conjugated IgG was used in separate control tubes. Fibrinogen binding was expressed as percentage of the increase in platelets binding fibrinogen compared with unactivated controls. Platelet activation by ADP was confirmed by expression of P selectin. No differences were noted in expression between null and WT platelets. Platelet activation during collection or processing in vitro was assumed to have occurred when the P selectin expression in unstimulated platelets exceeded 5%, and these samples were excluded from analysis.

Platelet lysis, GST pulldowns, and immunoprecipitation. Purified human platelets were handled and lysed as described (7). The entire cytoplasmic tail of TLT-1 was amplified by PCR and cloned into the pGEX-2TK vector (Amersham Biosciences; GE Healthcare). Fusion proteins were generated in BL-21 *Escherichia coli* and prebound to GST beads (Amersham Biosciences; GE Healthcare). Lysates were incubated with preloaded beads for 1–2 hours at 4°C, then washed with lysis buffer, and bound proteins were eluted with SDS-PAGE sample buffer. Immunoprecipitation and Western blotting were with anti–TLT-1 (svFv C10), anti-V5 monoclonal antibody (Invitrogen), anti-GFP (Abcam), anti-ezrin and anti-radixin (Sigma-Aldrich), or anti-moesin (NeoMarkers; Lab Vision, Thermo Scientific).

Peptide sequencing. Protein bands were excised from Coomassie-stained gels and digested with bovine sequencing grade trypsin (Roche). The extracted peptides were purified using μC18 ZipTip pipette tips (Millipore). Peptides were eluted with 1 μl solution containing 2 mg/ml of α-cyano-4-hydroxycinnamic acid in acetonitrile–0.1% trifluoroacetic acid (50/50 v/v). The purified peptides were spotted on target and analyzed by MALDI-TOF mass spectrometry. A Voyager-DE Pro mass spectrometer (Perceptive Bio-Systems) was used for analysis. The instrument was operated in a positive reflector mode. The accelerating voltage was 20 kV, guide wire was 0%, and grid voltage was 76%. The instrument was operated in reflector mode under positive ion conditions. A nitrogen laser was used at 337 nm, with 150 laser shots averaged per spectrum. Calibration was performed internally using trypsin autolytic peptides. Data analysis was carried out using Data Explorer software, version 4.3, resident on the instrument. Peptide mass lists were used to search the Swiss-Prot database with Mascot search engine (http://biospec.nih.gov/) with the following settings: taxonomy, human; missed cleavage, 1; peptide mass tolerance, 100 ppm.

Construction of the Treml1-null mouse. We flanked a neo cassette with approximately 250 base pairs of DNA sequence homologous to the sequences 3′ and 5′ prime to exons 1 and 2 of *Treml1*, and the cassette was inserted into a C57BL/6-derived BAC containing the entire *Treml1* gene as described (36). This construct was designed to completely prevent the expression of the TLT-1 protein by deleting the leader sequence as well as the splice sites for exons 1 and 2. BACs carrying the modification were screened by PCR using the 3-primer system (described below) and confirmed by Southern hybridization analysis and sequencing of the modified BAC PCR products. The resulting BAC-derived targeting vector contained approximately 190 kb of isogenic homologous flanking arms. The modified BAC was digested with *Not*I, phenol chloroform extracted, and electroporated into C57BL/6J mouse embryonic stem cells. 96 clones were picked for analyses; 12 clones were screened by fluorescent in situ hybridization as described by Seed et al. (37). We used the whole unmodified BAC as a probe yielding 7 positives. Clones showing only 2 points of hybridization by the probe were chosen for further evaluation (Supplemental Figure 1A). Their genomic structure was confirmed by Southern hybridization to *Kpn*I- or *Eco*RI-digested DNA using upstream and downstream genomic and neo probes (Supplemental

Figure 1B). The chosen clone (no. 5) was further confirmed by real-time PCR (data not shown). Positive clones were injected into BALB/c blastocysts and chimeric mice bred to C57BL/6J females to obtain heterozygotes in a pure C57BL/6 background. Heterozygous progeny were intercrossed to generate *Treml1*$^{-/-}$ mice. Three-primer PCR was carried out for genotyping tail DNA from offspring. Common forward primer 1 (5′-GGGGTACCTTGAGAATCAGATGGCCCTG-3′) was located at 5′ of the pgk-neo cassette; reverse primer 2 (5′-CGGCACATGTGGCAGCTCGTCCATGCCGAGAGTG-3′) was neo cassette specific, and reverse primer 3 (5′-GATCATCCTGCCTACAGTGG-3′) was WT specific. The PCR products were 1247 base pairs (mutant) and 942 base pairs (WT) (Figure 6). Absence of the TLT-1 protein was determined by Western blot and confocal analysis using rabbit polyclonal antibodies developed by this laboratory (6, 7).

Blood counts. Whole blood was collected via cardiac puncture. Platelet and leukocyte counts were determined using a Sysmex KX-21 Automated Hematology Analyzer Cell.

Platelet aggregation. Blood was isolated by cardiac puncture from mice anesthetized with CO_2 using a syringe containing 3.8% sodium citrate and spun at 100 *g* for 10 minutes to remove red cells. Blood from 3 to 5 mice of the same genotype was pooled. The final platelet count was adjusted to 2×10^8/ml, with platelet-poor plasma from the same mice. For washed platelets, platelet-rich plasma was spun at 2,100 *g* for 8 minutes; the platelets were washed in 10% acid citrate dextrose in Tyrode's buffer and were resuspended in Tyrode's buffer with 0.02 units/ml of aparase. Human platelets were prepared as described (10). Aggregation was initiated, with various agonists applied to a 400-μl aliquot at 37°C with stirring at 800 rpm and measured in a Chrono-log Corp. aggregometer. For the recombinant TLT-1 studies, rsTLT-1 was incubated with the platelets at least 3 minutes with stirring before the addition of agonist.

TNF and D-dimer analysis. Plasma was isolated by cardiac puncture as described in platelet aggregation studies. Plasma samples were frozen and later analyzed for mouse TNF (TNF-α ELISA; U-CyTech Biosciences; ANIARA), human D-Dimers (D-dimer ELISA kit; Hyphen BioMed; ANIARA), or mouse D-dimers (ASSERACHROM D-DI; Stago) according to the manufacturers' instructions.

Protein production and peptides. rsTLT-1 as been described (9). Peptides used in this study were purchased from AnaSpec. TLT-1 peptide sequence was derived from aa 94–110 (LQEEDAGEYGCMVDGAR). The control peptide sequence was derived from previously published work on the TREM family members (TDSRCVIGLYHPPLQVY) (13).

Bleeding-time assays. The bleeding-time measurements were performed as described (38). In brief, tails were cut 2 mm from the end and immersed in PBS at 37°C. The bleeding time was defined as the time required for the stream of bleeding to cease. All experiments with excessive bleeding were stopped at 10 minutes by cauterizing the tail.

Shwartzman reaction. Animals were shaved in the priming region with electric clippers. A priming dose of *E. coli* LPS (100 μg in 100 μl of sterile PBS; Sigma-Aldrich; *E. coli*:LPS 0127:B8) was injected subcutaneously using a 27-gauge needle. Mouse recombinant TNF (0.3 μg in 100 μl sterile PBS; PeproTech) was injected subcutaneously at the same site 20–24 hours later. Lesions were observed 24 hours after the second injection, and tissues were harvested for staining. The lesions were scored by individuals blinded to the genotype of the mice, and the scores were graded from no lesion (0) to hemorrhagic necrosis (4) (see below). Lesion area was determined by measurement of length and width of each lesion.

Histology. The skin was fixed in 10% buffered formalin, and paraffin sections were stained with H&E. The sections were examined by light microscopy and scored for thrombosis, hemorrhage, and inflammatory cellular infiltrate on a scale of 0 to 4, in which 0 was no response. The thrombi were graded from 1 to 4 depending on the percentage of vessels occluded (10% to 25%, 26% to 50%, 51% to 75%, and most vessels). Small hemorrhages associated with less than 20% vessels were graded 1, and those associated with 21% to 50% were graded 2. Moderate hemorrhage limited to the dermis was graded 3, and widespread red blood cells in the tissues extending into the subcutaneous tissue were graded as 4. For the inflammatory infiltrate, grade 1 was assigned for few neutrophils surrounding a minority of vessels, grade 2 indicated many neutrophils surrounding a minority of vessels, grade 3 was used for many neutrophils surrounding majority vessels, and grade 4 indicated numerous neutrophils widely scattered in the field.

Statistics. Descriptive results of continuous clinical variables were expressed as mean ± SD. Nonnormally distributed values, as assessed by the Kolmogorov-Smirnov test, were reported as median (IQR). Correlations between sTLT-1 plasma concentration and clinical or biological parameters were investigated by using the Spearman test. sTLT-1 was also tested for its association with several variables by using the Mann-Whitney *U* test. The time course of sTLT-1 plasma level was assessed by ANOVA. Analyses were completed with StatView Software, version 5.0 (Abacus), and a 2-tailed $P < 0.05$ was deemed significant. Tail bleeding times were expressed as means ± SD. We used the paired, 2-tailed Student's *t* test to evaluate for statistical differences between control and test groups for bleeding times, hemorrhage analysis, and lesion areas. Serum TNF levels were compared using the Mann-Whitney test and D-dimer levels; white blood cell counts and platelet counts were tested using Student's *t* test. Survival after LPS challenge was tested using the log-rank test. Some analysis was completed with Prism software, version 5.01 (GraphPad Software). $P < 0.05$ was considered statistically significant.

Acknowledgments

The authors would like to thank the staff of the Protein and Nucleic Acid and Optical Imaging Facilities at Universidad Central del Caribe. This research was supported in part by the Intramural Research Program of the NIH, National Cancer Institute, Center for Cancer Research, and under contract N01-Co-12400. Additional funding was obtained through grants from the National Center for Research Resources (NCRR), a component of the NIH (2G12RR3035), the National Institute of General Medical Sciences (SC2GM081237), and the Aniara Corp. The content of this publication does not necessarily reflect the views or policies of the Department of Health and Human Services, nor does mention of trade names, commercial products, or organizations imply endorsement by the NIH or the US government.

Received for publication May 12, 2008, and accepted in revised form March 11, 2009.

Address correspondence to: Daniel W. McVicar, Cancer and Inflammation Program, National Cancer Institute at Frederick, Building 560/31-46, Frederick, Maryland 21702, USA. Phone: (301) 846-5163; Fax: (301) 846-1673; E-mail: mcvicard@mail.nih.gov.

1. Cohen, J. 2002. The immunopathogenesis of sepsis. *Nature.* **420**:885–891.
2. Goerge, T., et al. 2008. Inflammation induces hemorrhage in thrombocytopenia. *Blood.* **111**:4958–4964.
3. Klesney-Tait, J., Turnbull, I.R., and Colonna, M. 2006. The TREM receptor family and signal integration. *Nat. Immunol.* **7**:1266–1273.
4. Bouchon, A., Dietrich, J., and Colonna, M. 2000. Cutting edge: inflammatory responses can be triggered by TREM-1, a novel receptor expressed on neutrophils and monocytes. *J. Immunol.* **164**:4991–4995.
5. Bouchon, A., Hernandez-Munain, C., Cella, M., and Colonna, M. 2001. A DAP12-mediated path-

way regulates expression of CC chemokine receptor 7 and maturation of human dendritic cells. *J. Exp. Med.* **194**:1111–1122.
6. Washington, A.V., Quigley, L., and McVicar, D.W. 2002. Initial characterization of TREM-like transcript (TLT)-1: a putative inhibitory receptor within the TREM cluster. *Blood.* **100**:3822–3824.
7. Washington, A.V., et al. 2004. A TREM family member, TLT-1, is found exclusively in the alpha-granules of megakaryocytes and platelets. *Blood.* **104**:1042–1047.
8. Lu, Y.T., et al. 2006. Preparation and characterization of monoclonal antibody against protein TREM-like transcript-1 (TLT-1). *Hybridoma (Larchmt.).* **25**:20–26.
9. Gattis, J.L., et al. 2006. The structure of the extracellular domain of triggering receptor expressed on myeloid cells like transcript-1 and evidence for a naturally occuring soluble fragment. *J. Biol. Chem.* **281**:13396–13403.
10. Giomarelli, B., et al. 2007. Inhibition of thrombin-induced platelet aggregation using human single-chain Fv antibodies specific for TREM-like transcript-1. *Thromb. Haemost.* **97**:955–963.
11. Levi, M., and Ten, C.H. 1999. Disseminated intravascular coagulation. *N. Engl. J. Med.* **341**:586–592.
12. Voves, C., Wuillemin, W.A., and Zeerleder, S. 2006. International Society on Thrombosis and Haemostasis score for overt disseminated intravascular coagulation predicts organ dysfunction and fatality in sepsis patients. *Blood Coagul. Fibrinolysis.* **17**:445–451.
13. Gibot, S., et al. 2004. A soluble form of the triggering receptor expressed on myeloid cells-1 modulates the inflammatory response in murine sepsis. *J. Exp. Med.* **200**:1419–1426.
14. Nakamura, F., Amieva, M.R., and Furthmayr, H. 1995. Phosphorylation of threonine 558 in the carboxyl-terminal actin-binding domain of moesin by thrombin activation of human platelets. *J. Biol. Chem.* **270**:31377–31385.
15. Doi, Y., et al. 1999. Normal development of mice and unimpaired cell adhesion/cell motility/actin-based cytoskeleton without compensatory up-regulation of ezrin or radixin in moesin gene knockout. *J. Biol. Chem.* **274**:2315–2321.
16. Lankes, W.T., and Furthmayr, H. 1991. Moesin: a member of the protein 4.1-talin-ezrin family of proteins. *Proc. Natl. Acad. Sci. U. S. A.* **88**:8297–8301.
17. Brozna, J.P. 1990. Shwartzman reaction. *Semin. Thromb. Hemost.* **16**:326–332.
18. Barrow, A.D., et al. 2004. Cutting edge: TREM-like transcript-1, a platelet immunoreceptor tyrosine-based inhibition motif encoding costimulatory immunoreceptor that enhances, rather than inhibits, calcium signaling via SHP-2. *J. Immunol.* **172**:5838–5842.
19. Lehman, C.M., Wilson, L.W., and Rodgers, G.M. 2004. Analytic validation and clinical evaluation of the STA LIATEST immunoturbidimetric D-dimer assay for the diagnosis of disseminated intravascular coagulation. *Am. J. Clin. Pathol.* **122**:178–184.
20. Nurden, A.T., et al. 2008. Phenotypic heterogeneity in the Gray platelet syndrome extends to the expression of TREM family member, TLT-1. *Thromb. Haemost.* **100**:45–51.
21. Gamulescu, M.A., Seifert, K., Tingart, M., Falet, H., and Hoffmeister, K.M. 2003. Platelet moesin interacts with PECAM-1 (CD31). *Platelets.* **14**:211–217.
22. Fukata, Y., et al. 1998. Association of the myosin-binding subunit of myosin phosphatase and moesin: dual regulation of moesin phosphorylation by Rho-associated kinase and myosin phosphatase. *J. Cell Biol.* **141**:409–418.
23. Retzer, M., and Essler, M. 2000. Lysophosphatidic acid-induced platelet shape change proceeds via Rho/Rho kinase-mediated myosin light-chain and moesin phosphorylation. *Cell Signal.* **12**:645–648.
24. Nakamura, F., Huang, L., Pestonjamasp, K., Luna, E.J., and Furthmayr, H. 1999. Regulation of F-actin binding to platelet moesin in vitro by both phosphorylation of threonine 558 and polyphosphatidylinositides. *Mol. Biol. Cell.* **10**:2669–2685.
25. Andre, P., et al. 2002. CD40L stabilizes arterial thrombi by a beta3 integrin–dependent mechanism. *Nat. Med.* **8**:247–252.
26. Angelillo-Scherrer, A., et al. 2001. Deficiency or inhibition of Gas6 causes platelet dysfunction and protects mice against thrombosis. *Nat. Med.* **7**:215–221.
27. Podrez, E.A., et al. 2007. Platelet CD36 links hyperlipidemia, oxidant stress and a prothrombotic phenotype. *Nat. Med.* **13**:1086–1095.
28. Prevost, N., et al. 2005. Eph kinases and ephrins support thrombus growth and stability by regulating integrin outside-in signaling in platelets. *Proc. Natl. Acad. Sci. U. S. A.* **102**:9820–9825.
29. Haselmayer, P., Grosse-Hovest, L., von Landenberg, P., Schild, H., and Radsak, M.P. 2007. TREM-1 ligand expression on platelets enhances neutrophil activation. *Blood.* **110**:1029–1035.
30. Camerer, E., et al. 2006. Roles of protease-activated receptors in a mouse model of endotoxemia. *Blood.* **107**:3912–3921.
31. Subramaniam, M., et al. 1996. Defects in hemostasis in P-selectin-deficient mice. *Blood.* **87**:1238–1242.
32. Knaus, W.A., et al. 1991. The APACHE III prognostic system. Risk prediction of hospital mortality for critically ill hospitalized adults. *Chest* **100**:1619–1636.
33. Vincent, J.L., et al. 1996. The SOFA (Sepsis-related Organ Failure Assessment) score to describe organ dysfunction/failure. On behalf of the Working Group on Sepsis-Related Problems of the European Society of Intensive Care Medicine. *Intensive Care Med.* **22**:707–710.
34. McCabe, W.R., and Jackson, G.G. 1962. Gram-negative bacteremia. I. Etiology and ecology. *Arch. Intern. Med.* **110**:845–847.
35. Le, G., Jr., Lemeshow, S., and Saulnier, F. 1993. A new Simplified Acute Physiology Score (SAPS II) based on a European/North American multicenter study. *JAMA.* **270**:2957–2963.
36. Liu, P., Jenkins, N.A., and Copeland, N.G. 2003. A highly efficient recombineering-based method for generating conditional knockout mutations. *Genome Res.* **13**:476–484.
37. Yang, Y., and Seed, B. 2003. Site-specific gene targeting in mouse embryonic stem cells with intact bacterial artificial chromosomes. *Nat. Biotechnol.* **21**:447–451.
38. Offermanns, S., Toombs, C.F., Hu, Y.H., and Simon, M.I. 1997. Defective platelet activation in G alpha(q)-deficient mice. *Nature.* **389**:183–186.